The Study of Cavitation in HDPE Using Time Resolved Synchrotron X-ray Scattering During Tensile Deformation

K. Schneider,[*1] *S. Trabelsi,*[2] *N.E. Zafeiropoulos,*[1] *R. Davies,*[3] *Chr. Riekel,*[3] *M. Stamm*[1]

Summary: Real time synchrotron Small-Angle and Wide-Angle X-ray Scattering was performed during the tensile deformation of a high-density polyethylene copolymer. The changes of the structure in the crystalline and in the amorphous domains were followed during the three characteristic stages of the load-displacement curves: The elastic stage and the plastic range composed of the stage of the lowering load in the force-displacement-curve (yielding) and the strain hardening. Competitive phenomena like crystallite fragmentation and cavitation were found to occur simultaneously in the phase of lowering the load but at different length scale. We prove that the void formation occurs mainly during yielding. During strain hardening there was no further increase of the void volume fraction, only changes in void size.

Keywords: polyethylene (PE); small-angle X-ray scattering (SAXS); voids; wide-angle X-ray scattering (WAXS)

Introduction

Due to their importance the mechanisms of plastic deformation in semi-crystalline polymers have been the topics of interest for theoretical and experimental studies over the last 30 years[1–3]. The concurrence between several phenomena during plastic deformation complicates the task to follow separately the transformation processes of the crystalline and the amorphous domains in semi-crystalline polymers. Crystallographic transformations such as slip, twinning, dislocation and martensitic transformation occurring in the crystalline phase have been studied extensively[1,2]. There are many papers, which provide detailed knowledge of the crystallographic slips appearing in HDPE at the yield point[4–6]. It is often observed that the plastic deformation of semi-crystalline polymers causes a significant amount of cavitation, which contributes to the toughening of the polymers. However, few recent investigations provided semi-quantitative studies about the cavitation phenomena using synchrotron X-ray scattering[7–9] and transmission electron microscopy[10–12].

The high flux of synchrotron radiation enables to characterize in situ the cavitation phenomenon occurring during the tensile deformation of high-density polyethylene copolymer in relation with the crystalline transformation. The aim of this paper is to describe the occurrence of competitive mechanisms such as the crystal plasticity and the voids formation with a time resolution of 10 seconds.

[1] Leibniz Institute of Polymer Research Dresden, Hohe Strasse 6, 01069 Dresden, Germany
Tel. (+49) 0351 4658 296, Fax: (+49) 0351 4658 281
E-mail: schneider@ipfdd.de
[2] Forschungszentrum Karlsruhe GmbH, Institut für Synchrotronstrahlung, ANKA, Hermann-von-Helmholtz-Platz 1, 76344 Karlsruhe, Germany
[3] European Synchrotron Radiation Facility (ESRF), BP 220, F38043 Grenoble, France

Experimental Section

Sample Preparation

From a polyethylene copolymers with a linear bimodal molar-mass distribution

with 3.7 C_2H_5-branches per 1000 C, $M_w = 3.3\ 10^5$ (HOSTALEN GM5010T3 natur, further details, see Men et al.[13], sample 10) provided by Basell Polyolefins, plates with a thickness of about 0.6 mm were produced by compression moulding. From the plates, small disc-shaped specimens (Ø 6.5 mm) were cut. The specimens were prepared with the use of a DSC Q1000 (TA Instruments) apparatus by annealing the sample 20 minutes at 180 °C, cooling down to crystallisation temperature of 115 °C, at which the sample crystallizes during 1h, afterwards quenched to room temperature (PE10_1_115). For comparison specimen directly from the compression moulded plate were used (PE10_untr.).

For the **estimation of true stress-strain behaviour** tensile tests were performed on a custom-made deformation rig (using a device from Kammrath & Weiss), with measurements performed *offline* and *in-situ* during x-ray scattering. To localise the highest tensile stress at a well defined position of the sample a miniaturised waiseted specimen (double notched specimen with a notch radius of 1 mm and a width between the notches of about 1.12 mm) were used (mini-dumb bell specimen, see Fig. 1).

During the online-experiments the beam position on the sample was fixed at the centre of the deformation region during all tests, mid-way between the mounting grips. The grips move in opposite directions to keep the mid-position in place. A constant speed of 0.15 mm/min was used at the beginning of the tests. To accelerate the experiments the speed was incresased in the strain hardening region to 0.6 mm/min. All the components of the rig are PC-controlled with a sampling rate of 1 s for all experiments.

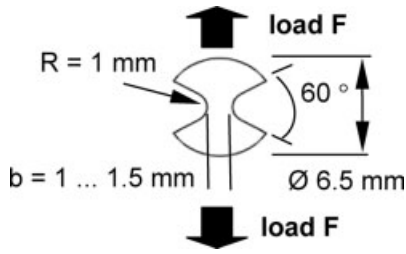

Figure 1.
Mini-dumb bell specimen.

A video camera took images from the specimen during test each 10 s in order to perform micro-deformation analysis by correlation (performed by the ARAMIS-software from GOM, Braunschweig). All the details of the equipment are described by Davies at al.[14].

Figure 2 shows engineering stress vs. displacement as well as true stress-strain curves of two different treated tensile specimen.

Four characteristic points (O, Y, S, F) displayed on the force-displacement as well on the true stress-strain curve are defined as

O: the starting point of the tensile deformation,
Y:the yielding point with a strain $\varepsilon_Y \approx 0.05$, (the stress is strongly dependent on the strain rate)
S: the beginning of the strain hardening at a strain of $\varepsilon_S \approx 3.0$,
F: the fracture point $\varepsilon_F \approx 6$ (strongly dependent on the individual specimen)

It is noticeable that despite the differences in the force-displacement-curves the true stress-strain-curves are quite similar. In the following sections, the mechanisms of the structural transformations occurring during the tensile deformation are discussed in the following regimes [O-Y], [Y-S] and [S-F].

Time resolved synchrotron WAXS and SAXS during the tensile deformation were carried out at the European Synchrotron Radiation Facility (ESRF) on the micro-focus beam line (ID13). A wave length of $\lambda = 0.98$ Å and beam spot-size of approximately 5 μm were used. In order to access to a large wave vector range two different configurations for the scattering experiments WAXS/SAXS and high resolution SAXS (HR-SAXS) were applied.

For data collection a MARCCD detector was used with a sample-to-detector distance of 171 mm for WAXS/SAXS.

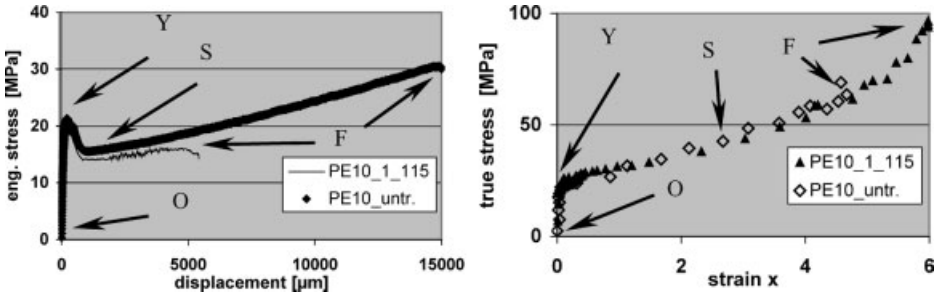

Figure 2.
Engineering stress-displacement curve (left) and true stress-strain curve (right) of PE10 (untreated and after thermal treatment 1 h at 115 °C). O refers to the starting point, Y to the yielding point, S to the begin of strain hardening, F to the fracture.

Diffraction patterns were generated each 11 s using an exposure time of about 1 s. For the HR-SAXS for voids investigation a sample-detector distance of 1044 mm was used to cover the wave vector range $0.08\ nm^{-1} \leq q \leq 0.8\ nm^{-1}$.

Data Analysis

The treatment of the WAXS and SAXS data was performed using the Fit2D[15] software application to correct the fluctuation of the incident beam intensity I_0 and to perform background subtraction as well as integration. The intensity profiles I(q) of the WAXS measurements were estimated using an azimuthal integration angle ψ in the range $180° \leq \psi \leq 360°$ outside the shadow of the beam stop.

For the SAXS data the meridional intensities $I^{MR}q^2$ (parallel to the stretching direction), where estimated in the range of $85° \leq \psi \leq 95°$, equatorial intensities $I^{EQ}q^2$, in the range of $-5° \leq \psi \leq 5°$.

Results and Discussion

In figure 3, WAXS/SAXS patterns acquired in-situ during the tensile deformation of PE10_1_115 until the fracture are shown. In the elastic regime [O-Y], no orientation effect has been detected; the SAXS pattern displays an isotropic scattering while the WAXS reflections are in the shape of rings. At the yielding point [Y], a new reflection with non-homogenous intensity appears which announce the starting of a transformation in the crystalline structure, it becomes intense in the region [Y-S] as the strain increases. This phenomenon is referred as the stress-induced martensitic transformation where the orthorhombic structure of undeformed PE is converted to the monoclinic structure in the deformed PE as it was described firstly as by Tanaka et al.[16] and confirmed later by other studies[5,7].

In the plastic deformation regimes [Y-S] and [S-F], the stretching of the sample leads to elongated SAXS patterns in the equatorial direction and to crystalline reflections with reduced azimuthal angle. For the highly deformed sample very close to the fracture, SAXS pattern could be assimilated to a streak and WAXS pattern to a fibre-like diffraction pattern.

Figure 4 displays the WAXS and SAXS scattering profiles corresponding of the **elastic region [O-Y]**. Short before the yielding point Y, the unique reflection (001) of the monoclinic crystalline system appears in the WAXS profile (see Figure 4, left). At the same time, in the meridional intensities $I^{MR}q^2$ of the SAXS, a slight shift of the second order correlation peak at $q \approx 0.52\ nm^{-1}$ to lower q occurs. This shift reflects the beginning of an increase in the long period $L = 2\pi/q$ probably due to the interlamellar separation. The long period L_M determined by the correlation function[17] is in the range of 20–25 nm.

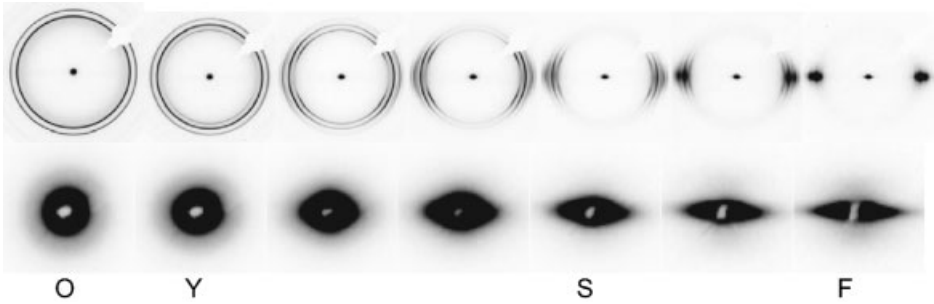

Figure 3.
Online WAXS/SAXS pattern of PE10_1_115 in the range [O-Y-S-F] with certain intermediate values.

Additionally, the increase in the intensities of the monoclinic peak (001), (200) is accompanied by a decrease in intensities of the orthorhombic peaks (110) and (200). Such an effect has been measured also by Butler et al. in drawn HDPE[7].

In the **first stage [Y-S] of the plastic regime**, an increase of the strain above the yielding point Y ($\varepsilon \approx 0.05$) leads to an opposite variation in the crystalline intensity of the orthorhombic and in the monoclinic structures (Figure 5, left side). The stress-induced martensitic transformation, which starts before the yielding point Y, leads to a monotone increases in the population of the crystallites having a monoclinic structure. However, in the second phase [S-F], the crystalline intensity of all the reflections decreases as function of the strain. Moreover, the full width at half maximum of the different crystalline peaks enlarges indicating a thinning of the crystallites in the equatorial direction ($\perp$ to the stretching direction) (Figure 5, right side). This result supports the occurrence of a melting of the crystallites. Figure (3) shows a remarkable diminution in the azimuthal angle $\Delta\psi$ of the equatorial reflections of the WAXS pattern in the phase [S-F] as consequence of crystallites alignment along the drawing direction.

Figure 6 shows the equatorial and the meridional SAXS intensity profiles $I^{EQ}q^2$ and $I^{MR}q^2$ respectively, recorded during tensile deformation between the yield point and the start of strain hardening $\varepsilon \in [Y–S] = [0.05–3.0]$.

The evolution of the first correlation peak of the crystallites at $q \approx 0.22\ nm^{-1}$ can be followed. The second correlation peak is noisy by comparison with first peak, the short exposure time does not enable to record both correlation peaks with comparable statistic.

The first correlation order in the intensity profiles becomes broader and weak with the deformation in the phase [Y-S] (Figure 6). It shifts to higher values in equatorial and to lower values in meridional direction with increasing strain.

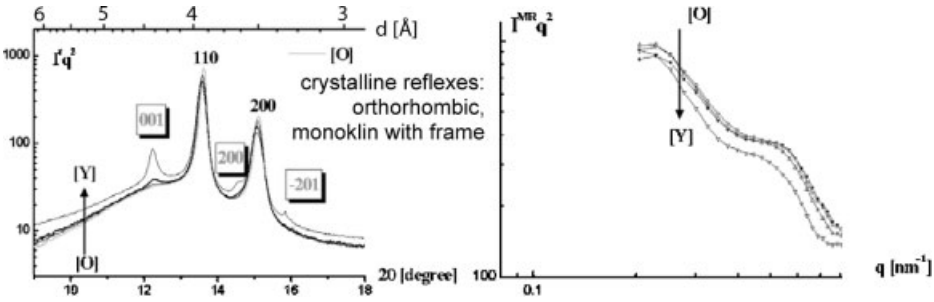

Figure 4.
WAXS- and SAXS-profiles of PE10_1_115 from the start of deformation to the yielding point Y.

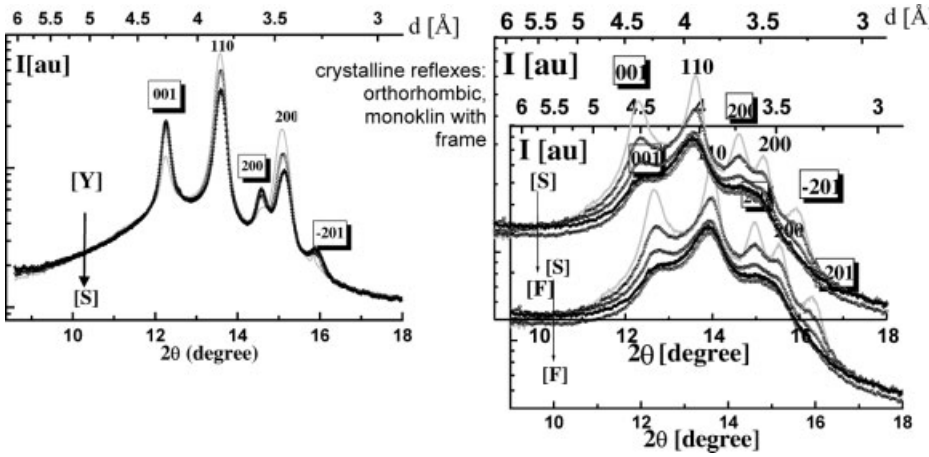

Figure 5.
WAXS-profiles of the plastic region [Y-S] (left) and [S-F] (right) of PE10_1_115.

In the direction transverse to the drawing direction (Figure 6, left), the equatorial long spacing disappears and the intensity profile $I^{EQ}q^2$ displays rather a diffuse scattering.

Apart form the crystallographic transformation, the amorphous phase undergoes stress-induced changes due to **cavitation phenomena** in the plastic regime [Y-S] and [S-F], which can be detected mainly from the variation of SAXS profiles as function of the strain.

After the yielding point, the total scattered intensity of the PE10 sample increases gradually due the formation of the voids, exceptionally at low q-values. Such effect could be explained by the presence of an increasing number of voids on a length scale in the order of 70 nm or more. The onset of cavitation does not seems do coincide with the onset of the martensitic transformation as it was mentioned in other studies[7].

The monotonically changing slope of SAXS profiles in the meridional and the equatorial directions in the wave vector range $0.08\ nm^{-1} \leq q \leq 0.2\ nm^{-1}$ as well as the ratio between both informs about a continuous change in the size and in the shape of the cavities.

In the first region of yielding the ratio $I^{MR}(\varepsilon)/I^{EQ}(\varepsilon)$ of the meridional intensity to the equatorial intensity increases with strain. Furthermore, for $\varepsilon = [0.05–0.4]$ the meridional intensity $I^{MR}(\varepsilon)$ is higher than the equatorial one $I^{EQ}(\varepsilon)$ especially for the small q values. This means that the voids

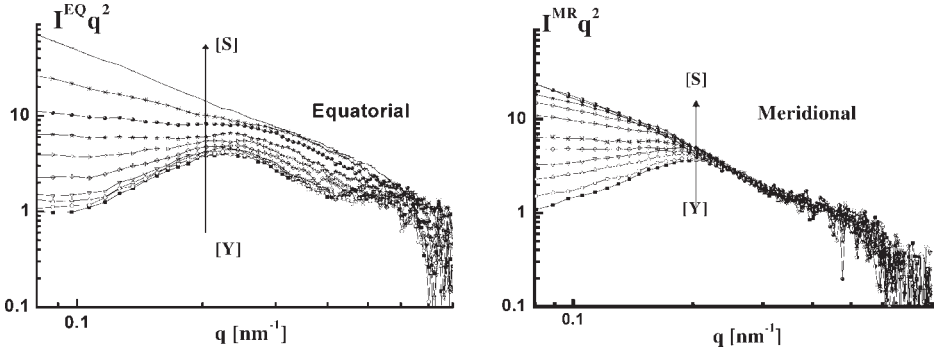

Figure 6.
Equatorial and meridional SAXS-profiles of the plastic range [Y-S] of PE10_1_115.

are firstly extended in the transverse to the drawing direction. However, with increasing strain the trend is inversed, indicating that the voids becomes more elongated in the stretching direction.

Beyond the yielding region, in the phase of **strain hardening [S-F]** the SAXS profiles do not vary significantly. The decrease in the meridional intensity $I^{MR}q^2$ is accompanied by a slight increase in the equatorial intensity $I^{EQ}q^2$ (Figures 7). While the decrease of $I^{MR}q^2$ can be understood at least partially as a measure of decreasing sample thickness, the decrease of the ratio $I^{MR}q^2/I^{EQ}q^2$ by a factor of about 10 is again a hint on the ongoing orientation effect parallel to stretching direction as well as a further stretching of the cavities.

Synopsis

Several features of the processes of plastic deformation were derived from time resolved WAXS/SAXS measurements including the formation of the voids and their deformation with strain in the plastic regime [Y-F]. It should be described through the sketch in Figure 8. In the literature[8,9], few schematic illustrations of the development of the cavities are recently presented. Figure 8 displays a sketch partially extracted from the model of Shultz[18], which describes the different steps of deformation for crystalline lamellae in diagonal regions. In this model, the phenomenon of cavitation was not taken into account and discussed. We suggest to describe the deformation mechanism in steps, which involves several processes modes.

In the **elastic regime** [O-Y] a slight shift in the first and second order correlation peak is probably correlated with interlamellar separation. Very close to the yielding point, SAXS pattern appears anisotropic rather than circular indicating the incipient orientation of the lamellar stacks in the stretching direction (Figure 8b).

In the first phase of yielding (up to about $\varepsilon = 0.4$) the long period vanishes progressively. Simultaneously an increase in the scattering power intensity occurred due to the increase of the volume fraction of the voids in the material is observed. The appearance of the cavities is strongly coupled with the disappearance of the long spacing through the break-up of the lamellar stack. The shearing mode suggested by Peterlin[19] to describe the lamellar fragmentation into crystalline blocks appeared to be convincing process. The increase of the intensity with the strain supports that the voids are firstly extended in the transverse direction to the draw direction as illustrated in Figure 8c.

In the second phase of the yielding (about from $\varepsilon = 0.4$ to $\varepsilon = 3.0$) the voids should be elongated in the stretching direction. Moreover, the SAXS profiles display power law decay due to the destruction of the lamellar stack in the equatorial and in the meridional directions.

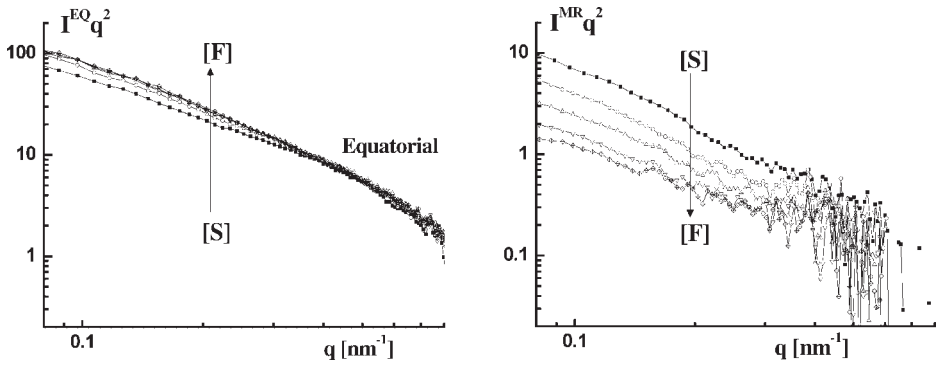

Figure 7.
Equatorial and meridional SAXS-profiles of PE10_1_115 during strain hardening to failure.

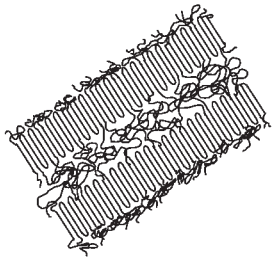

a) Lamellar stacks oriented in the diagonal direction

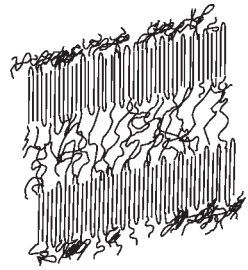

b) orientation of the lamellar stacks along the stretching direction and lamellar separation

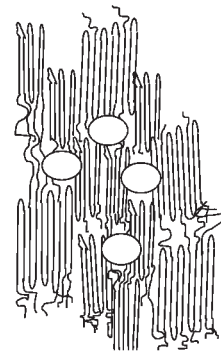

c) lamellar fragmentation into microblock crystallites during the phase [Y-S] which leads the formation of the voids elongated ⊥ to the stress

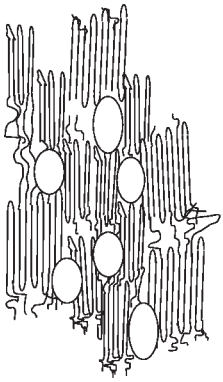

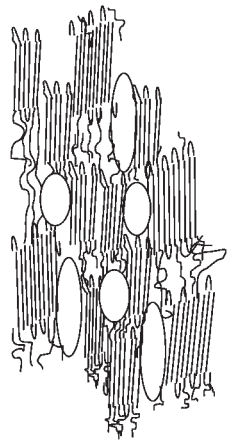

d) increase in the volume fraction of the voids during force release after the yielding point [Y-S], by d_1) the formation of the voids elongated ⊥ to the stress (left) d_2) increase in the size of the voids in both directions (right)

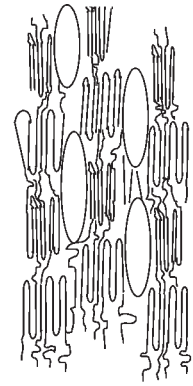

e) elongation of voids and stretching of chains also in the amorphous phase in meridional direction and decrease of the crystallite dimensions

Figure 8.
Schematic illustrations of the different transformation steps (see text).

Therefore, no long period spacing should be expected in both directions, (see Figure $8d_1$, $8d_2$).

The phase of strain hardening is mainly characterised further stretching of crystallites and voids and the successive dissolution of the crystallites. Despite distinct crystalline reflexes a rather broad intensity peak remains in the region of the reflexes. This indicates a high orientation of the chains also at declining crystalline order. The constancy of the total intensity with the strain in the range of smaller wave vector $\mathbf{0.08\ nm^{-1} \leq q \leq 0.2\ nm^{-1}}$ indicates that the volume fraction of the voids does not alter. Only the size of the voids in the phase becomes more oriented (see Figure 8e).

Conclusion

Elastic and plastic deformation mechanisms in a polyethylene copolymer were studied in tension using in-situ time

resolved synchrotron radiation x-ray scattering. In the plastic deformation phase, cavitation phenomena were found to occur in tension simultaneously with the changes in crystalline order, crystallite fragmentation or crystallite dissolving but at different length scale.

Moreover, we deduced from the intensity variation that the voids were firstly extended in the transverse to the draw direction and became elongated along the stretching direction as the strain increases.

In the strain-hardening region [S-F], no further changes in the volume fraction and in the size of the voids have been detected. The increase of the strain led only to the establishment of new ordering of the microblocks crystallites, which became highly oriented and with further strain successive dissoluted.

A publication of a more detailed evaluation of the presented data as well as the extension of the technique to other grades of PE as well as other geometries, e.g. the fracture mechanical EWF test, is in preparation.

Acknowledgement: The authors would like to thank Manfred Burghammer from ESRF, beam line ID13 for the support during the experiments undertaken as part of a long-term proposal (SC-1099). Support of this work and providing the materials by BASF Aktiengesellschaft, Polymer Physics, 67056 Ludwigshafen, Germany, is gratefully acknowledged. We would like to thank Ms. J. Henle for assisting with the experiments.

[1] Bowden. PB., Young. R.J., *J. Mater. Sci*, **1974**, 9, 2034.
[2] Haudin. JM, in *Plastic deformation of amorphous and semi-crystalline materials*, Escaig. B, G'Sell. C, eds, Paris: Les éditions de Physique; **1982**, p291.
[3] Peterlin. A.; *J. Mater. Sci*, **1971**, 6, 490.
[4] Bartczak. Z., Argon. A.S, Cohen. R. E., *Macromoelcules*, **1992**, 25, 5036.
[5] Bartczak Z.; Cohen. R. E.; Argon A.S., *Macromoelcules*, **1992**, 25, 4692.
[6] Galeski. A.; Bartczak. Z.; Cohen R. E.; Argon A.S.;, *Macromoelcules*, 1992, 25, 5705.
[7] Butler. M. F., Donald. A. M., Bras. W., Mant. G. R., Derbyshire. G. E., Ryan. A. J., *Macromelcules*, **1995**, 28, 6383.
[8] Butler. M. F., Bonald. A. M., Ryan. A. J., *Polymer*, **1998**, 39, 39.
[9] Men. Y., Rieger. J., Homeyer. J. *Macromecules*, **2004**, 37, 9481.
[10] Michler G. H., Godehardt. R., *Cryst. Res. Technol*, **2000**, 35, 863.
[11] Michler. G. H., *Colloid. Polym. Sci*, **1992b**, 270, 627.
[12] Galeski. A., Argon. A.S., Cohen R. E., *Macromoelcules*, **1989**, 21, 2761.
[13] Men. Y. E., Rieger. J., Enderle. H.-F., Lilge. D., *Eur. Phys. J. E*, **2004**, 15, 421.
[14] Davies R.J, Zafeiropoulos N.E, Schneider K, Burghammer M, Riekel. C, Kotek. J.C., Stamm. M. *Colloid. Polym. Sci*, **2004**, 282, 854.
[15] http://www.esrf.fr/computing/scientific/FIT2D/
[16] Tanaka. K., Seto. T., Hara. T. J. Phys. Soc. Jpn. **1962**, 17, 873.
[17] Santa Cruz. C, N. Stribeck, Zachmann. H. G., Macromelcules, **1991**, 24, 5980.
[18] Schultz. J. M., Polym. Mater. Sci, Prentice-Hall, Englewood Cliffs, **1974**, p 496–499.
[19] Peterlin. A., Kolloid zuz Polymere, **1969**, 233, 857.

